# Ka-

# BAND

## Standoff Through-wall Sensing at Ka-band

by S. Liao, T. Elmer, S. Bakhtiari, N. Gopalsami, N. Cox, J. Wiencek and A.C. Raptis

Recently, microwave standoff/remote through-wall imaging (TWI), or sensing, has attracted a considerable amount of interest (Aamna et al., 2010; Aftanas et al., 2008; Aftanas, 2009; Ahmad et al., 2008; Dehmollaian and Sarabandi, 2006; Johnson et al., 2009; Yemelyanov et al., 2009). The long-range and penetrative nature of a microwave through optically opaque dielectric materials makes it an ideal candidate for TWI of distant or inaccessible objects with the required spatial resolution.

Conventional microwave remote TWI of objects made of different materials is usually performed at frequencies below 3 GHz that provide relatively low spatial resolution. In this paper, the authors evaluate the ability and sensitivity of high-frequency microwave or millimeter wave standoff sensing of through-wall objects to achieve high spatial resolution. The target under study was a sandwich structure consisting of different object materials placed between

Through-wall searching and identification of human subjects is of great interest for many purposes two wall blocks. A vector network analyzer (VNA) was used to sweep over the entire Ka-band (26.5 to 40 GHz). The beam was then directed to a standard rectangular horn antenna and collimated by a 152 mm (6 in.) diameter Gaussian lens towards the sandwich structure of wall block/object/wall block. The reflected electromagnetic wave was picked up by the same system as the complex *S*-parameter, $S_{11}$. Both amplitude and phase of the reflected signal were used to recognize different materials sandwiched between the cement blocks. The experimental results were compared with the theoretical calculations, which show satisfactory agreement for the cases evaluated in this work.

### Potential Applications

The penetration property of the electromagnetic wave has found various industrial, civil and military applications (Botros et al., 1984; Chen et al., 2000; D'Urso et al., 2009; Lubecke et al., 2007; Pieraccini et al., 2008; Sen et al., 2002; Zhuravlev et al., 2011). Various techniques at different frequency ranges have been explored extensively in the past few decades. Most investigations were performed at the lower frequency range of microwaves, that is, from direct current to 3 GHz. This is because a microwave attenuates less in this frequency range and in turn provides larger penetration depth (Yemelyanov et al., 2009). Furthermore, there are commonly three operation modes: continuous wave, frequency-modulated continuous wave (FMCW) and pulse. Typical applications of TWI can be separated into three categories: human inside building, buried humans and hidden object inspection.

### Human inside Building

Through-wall searching and identification of human subjects is of great interest for many purposes, which include searching for trapped human subjects after disasters such as fires, flooding and tornados; terrorists or hostages inside enclosed structures during counter-terrorism or rescue operations; and soldiers in the battlefield. For example, through-wall vital sign detection and monitoring using an ultra-wide band radar signal have been investigated, and X-band continuous wave radar has been studied in previous works (D'Urso et al., 2009; Lubecke et al., 2007).

### Buried Humans

Searching for buried humans is an important application of TWI. Typical examples are: buried humans under rubble after earthquakes; buried humans under snow after an avalanche; and humans hidden or lost inside a forest. For example, in a previous study, ultra-high frequency-band and L-band continuous wave radars were used to detect human subjects buried under simulated earthquake rubble; also, S-band radar was used to detect buried human subjects during snow avalanches in another study (Chen et al., 2000; Pieraccini et al., 2008).

### Hidden Object Inspection

The penetration property of the electromagnetic wave can be used for noncontact inspection applications such as: hidden objects inside walls; buried landmines, cables and pipes; and underground structures such as soil, rock stratigraphy, ice depth and hidden tunnels for illegal immigration and transport of illicit materials. For example, one study used L-band FMCW radar for detection of hidden objects inside walls; another study investigated an S-band/C-band /Ku-band continuous wave radar for detection of under-surface hidden objects; and a third study used a very-high frequency airborne pulse radar for remote sensing of underground buried objects (Botros et al., 1984; Sen et al., 2002; Zhuravlev et al., 2011).

### Contribution of this Paper

One disadvantage of low-frequency microwaves is their relatively low spatial resolution limited by the diffraction effect of electromagnetic waves. Higher-frequency microwave techniques have also been investigated by other researchers, primarily for nondestructive testing of layered materials (Bakhtiari et al., 1994; Bakhtiari et al., 1995; Bois et al., 2000; Mubarak et al., 2001; Zoughi et al., 1995). Those studies, on the other hand, have been limited mostly to measurements over a relatively narrow band. This paper investigates TWI at the upper end of the microwave and the lower end of the millimeter wave (mmW) spectrum, covered by the Ka-band (26.5 to 40 GHz), aimed at achieving higher spatial resolution. Experimental sensing of various materials sandwiched between two cement blocks in the Ka-band was compared with the theoretical calculations to validate the feasibility of standoff TWI ability at such a high frequency range.

## Experimental Setup

The experimental setup used to investigate the concept of mmW TWI is shown in Figure 1. The microwave apparatus consisted of a four-port VNA for stepping through frequencies from 26.5 to 40 GHz; a Ka-band standard rectangular horn antenna; and a 152 mm (6 in.) diameter Gaussian horn antenna for collimating the beam. The plane wave propagated towards a sandwiched structure, which was perpendicular to the beam path and was located approximately 762 mm (30 in.) away from the lens. The reflected wave was picked up by the same Ka-band horn antenna and was processed by the VNA to determine

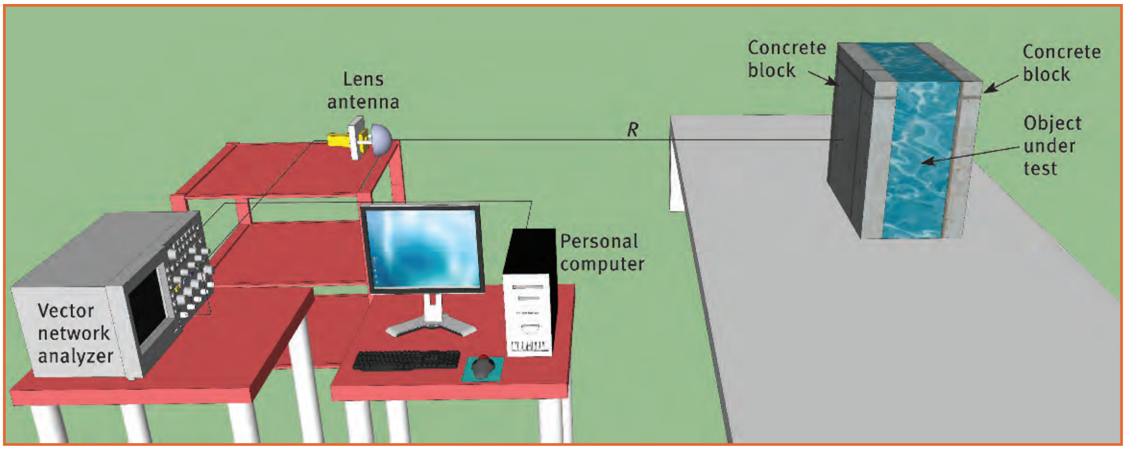


**Figure 1. Experimental setup for the standoff through-wall sensing of different objects: water, soil, rocks and metal. The object was placed between two wall blocks forming a sandwich structure. The measurement range is denoted by *R*.**

the complex $S_{11}$ parameter (reflection coefficient). The sandwich structure was composed of two wall blocks of 35.6 mm (1.4 in.) thick cement with 178 mm (7 in.) spacing where different materials could be placed. Commercial software running on a personal computer was developed to record the $S_{11}$ parameter and to further process the data.

## Theoretical Simulation

Figure 2 depicts the simplified numerical model of the experimental setup shown in Figure 1. Without loss of generality, in the far field region the collimated beam can be approximated by an incident plane wave, which reduces the model to plane wave incidence upon a layered dielectric structure. The problem may then be readily solved through the boundary matching technique on all four interfaces separating different materials. In reference to Figure 2, from left to right, boundary #1 is the air/wall block interface, boundary #2 is the wall block/object interface, boundary #3 is the object/wall block interface and boundary #4 is the wall block/air interface. In reference to Table 1, the electric field (E-field) and the magnetic field (H-field) inside each of the three layers of the target structure can be expressed as forward and backward propagating waves, where $\gamma_w$ and $\gamma_0$ are wave propagation constants that include the attenuation effect inside the wall block and inside the object, respectively, and $r$, $\alpha$,

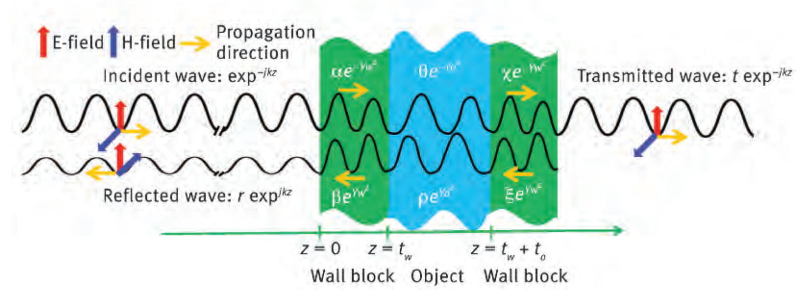


**Figure 2. Simplified model of plane wave propagation through the wall block/object/wall block sandwich structure.**

**TABLE 1**
**Total E- and H-field inside each region**

| Regions | #1: air | #2: wall block | #3: object | #4: wall block | #5: air |
|---|---|---|---|---|---|
| E-field | $e^{-jkz} + re^{jkz}$ | $\alpha e^{-\gamma_w z} + \beta e^{\gamma_w z}$ | $\theta e^{-\gamma_o z} + \rho e^{\gamma_o z}$ | $\chi e^{-\gamma_w z} + \xi e^{\gamma_w z}$ | $te^{-jkz}$ |
| H-field $\times j\omega\mu$ | $jk(e^{-jkz} - re^{jkz})$ | $\gamma_w(\alpha e^{-\gamma_w z} - \beta e^{\gamma_w z})$ | $\gamma_o(\theta e^{-\gamma_o z} - \rho e^{\gamma_o z})$ | $\gamma_w(\chi e^{-\gamma_w z} - \xi e^{\gamma_w z})$ | $jkte^{-jkz}$ |

In this experiment, 1601 frequencies evenly distributed between 26.5 and 40 GHz were recorded for all the measurement scenarios.

$\beta$, $\theta$, $\rho$, $\chi$, $\xi$ and $t$ are coefficients for each related wave component (Jackson, 1998). As shown in Table 2, the field equations at each interface may then be obtained by enforcing the continuity of both the E-field and the H-field at each boundary, where $k$ is the wave vector in the air; $t_w$ and $t_0$ are the thickness of the wall block and the object, respectively; and $\gamma_w$ and $\gamma_0$ are the propagation constant of the wall block and the object, respectively.

The equations in Table 2 can be readily solved using software for all eight unknowns ($r$, $\alpha$, $\beta$, $\theta$, $\rho$, $\chi$, $\xi$ and $t$) by using the eight boundary conditions. In matrix form, Table 2 reduces to the equations shown in Figure 3, where $f$ is the frequency and $\varepsilon_w$ and $\varepsilon_0$ are the dielectric constant of the wall block and the object, respectively.

The calculated results and their comparison with the experimental results will be discussed in the following sections.

## Experimental Result

In this experiment, 1601 frequencies evenly distributed between 26.5 and 40 GHz were recorded for all the measurement scenarios. The intermediate-frequency bandwidth of the VNA was set to 10 Hz in order to increase the signal-to-noise ratio, which is inversely proportional to the intermediate-frequency bandwidth.

## System Calibration

Because of the existence of background stray field, $E_b$, it was necessary to calibrate the measurement system. The measured $S$-parameter, $S_{11}$, can be expressed as follows:

$$(1) \quad S_{11} = \left(E_b + E_r\right)T(f) = E_i\left(r_b + r\right)T(f)$$

where

$E_b$, $E_r$ and $E_i$ are the background stray field, the reflected field due to the structure and the incident field, respectively,

$T(f)$ is the transfer function of the system (Liao et al., 2011).

The goal was to ultimately extract the true reflection signal, $r$, from the measurements. The $S$-parameter for the background, $S_{11}^b$, and the $S$-parameter for the reflection from a metal surface, $S_{11}^m$, which are measurable quantities, can be expressed as follows in Equations 2 and 3.

$$(2) \quad S_{11}^b = E_i r_b T(f)$$

$$(3) \quad S_{11}^m = E_i\left(r_b - 1\right)T(f)$$

From these two equations, one gets Equation 4.

$$(4) \quad E_i T(f) = S_{11}^b - S_{11}^m$$

By combining Equation 1 with Equation 4, the true reflection coefficient from the structure is then given by Equation 5.

$$(5) \quad r = \frac{S_{11} - S_{11}^b}{S_{11}^b - S_{11}^m}$$

## Dielectric Constant of Wall Block

In order to solve the equation in Figure 3, the dielectric constant of the wall block first had to be determined. This was obtained through direct measurement of the $S$-parameter, $S_{11}$, at 101 frequency points within the Ka-band for an individual wall

**TABLE 2**
**E- and H-field boundary conditions at each interface**

| Boundaries | #1: air/wall block | #2: wall block/object | #3: object/wall block | #4: wall block/air |
|---|---|---|---|---|
| E-field boundary condition | $1 + r = \alpha + \beta$ | $\alpha e^{-\gamma_w t_w} + \beta e^{\gamma_w t_w}$ $= \theta e^{-\gamma_o t_w} + \rho e^{\gamma_o t_w}$ | $\theta e^{-\gamma_o [t_w + t_o]} + \rho e^{\gamma_o [t_w + t_o]}$ $= \chi e^{-\gamma_w [t_w + t_o]} + \xi e^{\gamma_w [t_w + t_o]}$ | $\chi e^{-\gamma_w [2t_w + t_o]} + \xi e^{\gamma_w [2t_w + t_o]}$ $= t e^{-jk[2t_w + t_o]}$ |
| H-field boundary condition | $jk(1 - r)$ $= \gamma_w(\alpha - \beta)$ | $\gamma_w(\alpha e^{-\gamma_w t_w} - \beta e^{\gamma_w t_w})$ $= \gamma_o(\theta e^{-\gamma_o t_w} - \rho e^{\gamma_o t_w})$ | $\gamma_o(\theta e^{-\gamma_o [t_w + t_o]} - \rho e^{\gamma_o [t_w + t_o]})$ $= \gamma_w(\chi e^{-\gamma_w [t_w + t_o]} - \xi e^{\gamma_w [t_w + t_o]})$ | $\gamma_w(\chi e^{-\gamma_w [2t_w + t_o]} - \xi e^{\gamma_w [2t_w + t_o]})$ $= jkt e^{-jk[2t_w + t_o]}$ |

**(a)**

$$\overline{\overline{M}}(f,\varepsilon_w,\varepsilon_o,t_w,t_o)\times\bar{u}(\alpha,\beta,\theta,\rho,\chi,\xi)=\left[1;\,jk;0;0;0;0;0;0\right]^T$$

$$\overline{\overline{M}}(f,\varepsilon_w,\varepsilon_o,t_w,t_o)$$

$$=\begin{bmatrix} -1 & 1 & 1 & 0 & 0 & 0 & 0 & 0 \\ jk & \gamma_w & -\gamma_w & 0 & 0 & 0 & 0 & 0 \\ 0 & e^{-\gamma_w t_w} & e^{\gamma_w t_w} & -e^{-\gamma_o t_w} & -e^{\gamma_o t_w} & 0 & 0 & 0 \\ 0 & \gamma_w e^{-\gamma_w t_w} & -\gamma_w e^{-\gamma_w t_w} & -\gamma_o e^{-\gamma_o t_w} & \gamma_o e^{-\gamma_o t_w} & 0 & 0 & 0 \\ 0 & 0 & 0 & e^{-\gamma_o[t_w+t_o]} & e^{\gamma_o[t_w+t_o]} & -e^{-\gamma_w[t_w+t_o]} & -e^{-\gamma_w[t_w+t_o]} & 0 \\ 0 & 0 & 0 & \gamma_o e^{-\gamma_o[t_w+t_o]} & -\gamma_o e^{\gamma_o[t_w+t_o]} & -\gamma_w e^{-\gamma_w[t_w+t_o]} & \gamma_w e^{\gamma_w[t_w+t_o]} & 0 \\ 0 & 0 & 0 & 0 & 0 & e^{-\gamma_w[2t_w+t_o]} & e^{\gamma_w[2t_w+t_o]} & e^{-jk[2t_w+t_o]} \\ 0 & 0 & 0 & 0 & 0 & \gamma_w e^{-\gamma_w[2t_w+t_o]} & -\gamma_w e^{\gamma_w[2t_w+t_o]} & -jke^{-jk[2t_w+t_o]} \end{bmatrix}$$

**(b)**

**Figure 3. Equation (a) and matrix (b) derived from reducing Table 2. *f* is the frequency and *$e_w$ and $e_o$ are* the dielectric constant of the wall block and the object, respectively.**

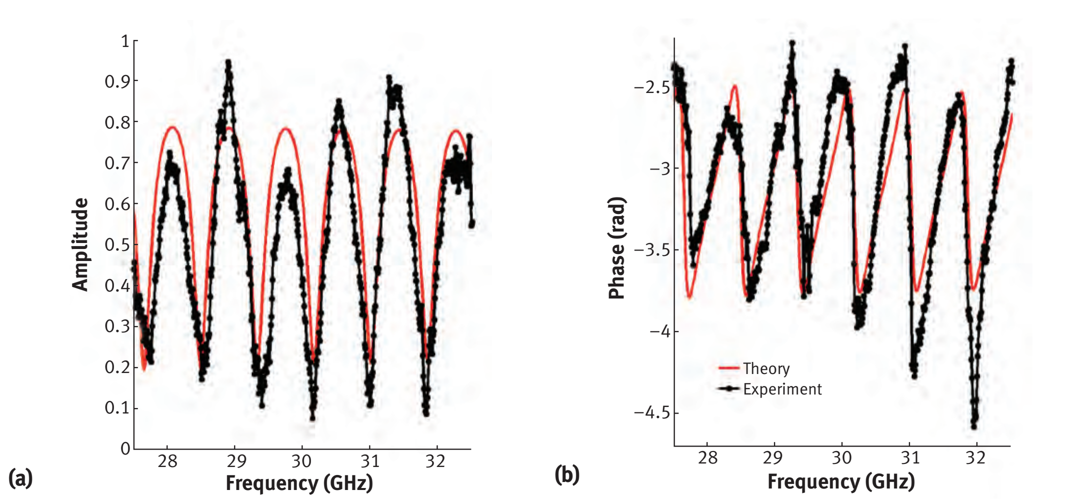


**Figure 4. Experimental reflection is fitted to theoretical calculation, that is, Equation 6, to obtain the dielectric constant of the wall block used in the experiment, which was determined to be $\varepsilon_w$ = 12.4(1 – *j*0.003): (a) amplitude; and (b) phase.**

block. The measurement data could then be fitted by using the following theoretical formula in Equation 6 (Liao et al., 2011).

$$r_w=\frac{\left[\frac{1}{\varepsilon_w}-1\right]\left[1-\exp\left(-j2k_w t_w\right)\right]}{\left[\frac{1}{\sqrt{\varepsilon_w}}+1\right]^2-\left[\frac{1}{\sqrt{\varepsilon_w}}-1\right]^2\exp\left(-j2k_w t_w\right)} \qquad (6)$$

Using this approach, an average value of $\varepsilon_w$ = 12.4(1 – *j*0.003) was obtained for the dielectric constant of the wall block. Comparison of the experimental result with that calculated using Equation 6 is shown in Figure 4.

### $S_{11}$ of the Sandwich Structure

The *S*-parameter, $S_{11}$, for the sandwiched water object is shown in Figure 5, together with the theoretical results calculated according to the equations in Figure 3. A snapshot of data in Figure 4 over a narrow

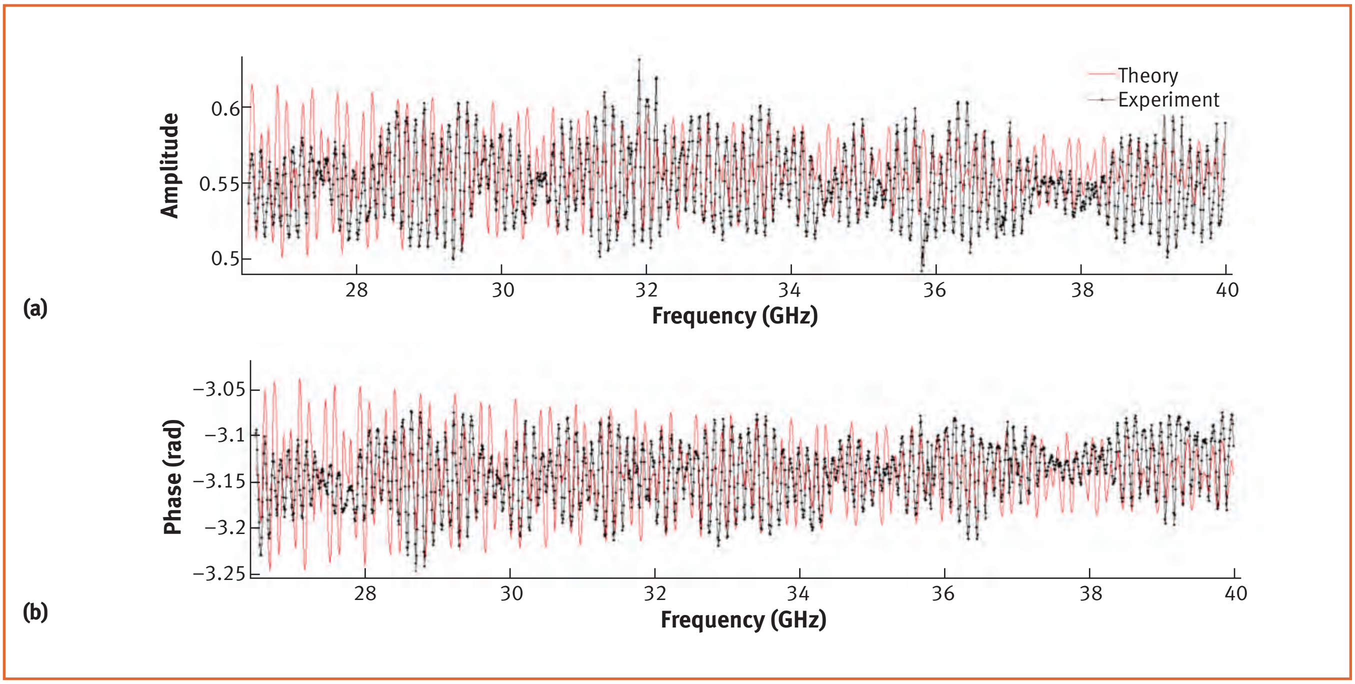


**Figure 5. Experimental and calculated *S*-parameter, $S_{11}$, for wall block/water/wall block sandwich structure, where $\varepsilon_W = 12.4(1 - j0.003)$ and $\varepsilon_O = 77$ for water: (a) amplitude; and (b) phase.**

frequency range is shown in Figure 6. The parameters used for fitting were $\varepsilon_W = 12.4(1 - j0.003)$, obtained from Figure 4, and water as the sandwiched object, with a dielectric constant $\varepsilon_O = 77$. The sandwich structure, *R*, was approximately 762 mm (30 in.) away from the antenna.

Following the validation of the procedure for extraction of dielectric properties of the test object, several experiments were carried out using different materials sandwiched between the two wall blocks, that is, soil, rocks and metal. To demonstrate the ability to see the contrast between different objects

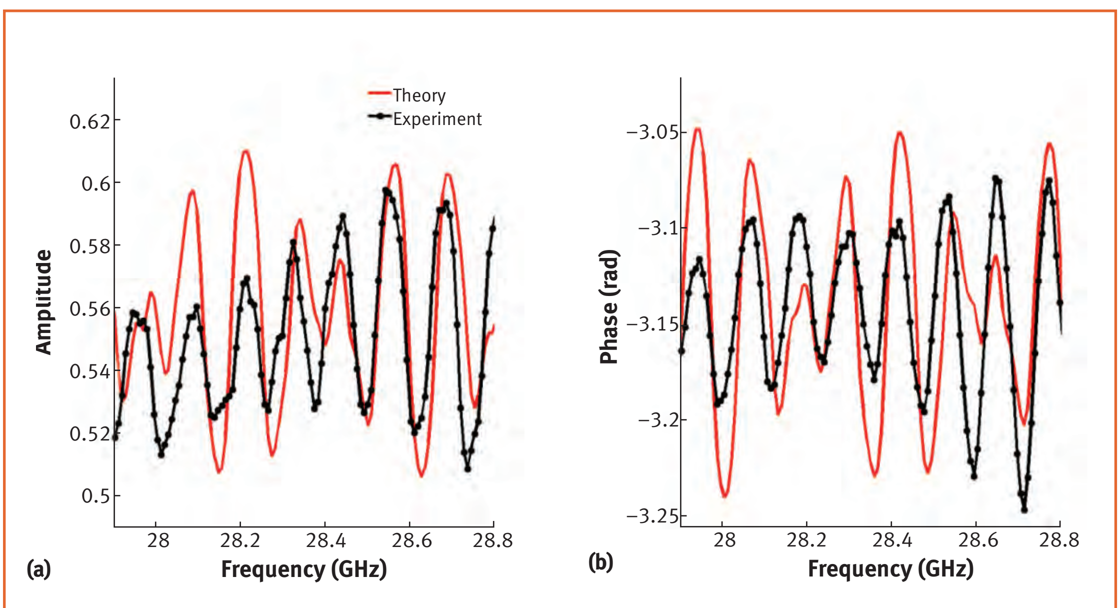


**Figure 6. A snapshot of Figure 4 to show the details over a narrow frequency range: (a) amplitude; and (b) phase.**

behind the wall, the difference (with that of water as the object) of the $S$-parameter, $\Delta S_{11} \equiv S_{11} - S_{11}$ (water), for three different materials is shown in Figure 7. Both the amplitude and the phase spectrum are displayed. Once again, Figure 8 provides a snapshot of Figure 7, allowing for a more detailed observation of the data over a narrow bandwidth. From the $S$-parameter contrast, one can clearly distinguish different materials by combining both the amplitude and the phase information.

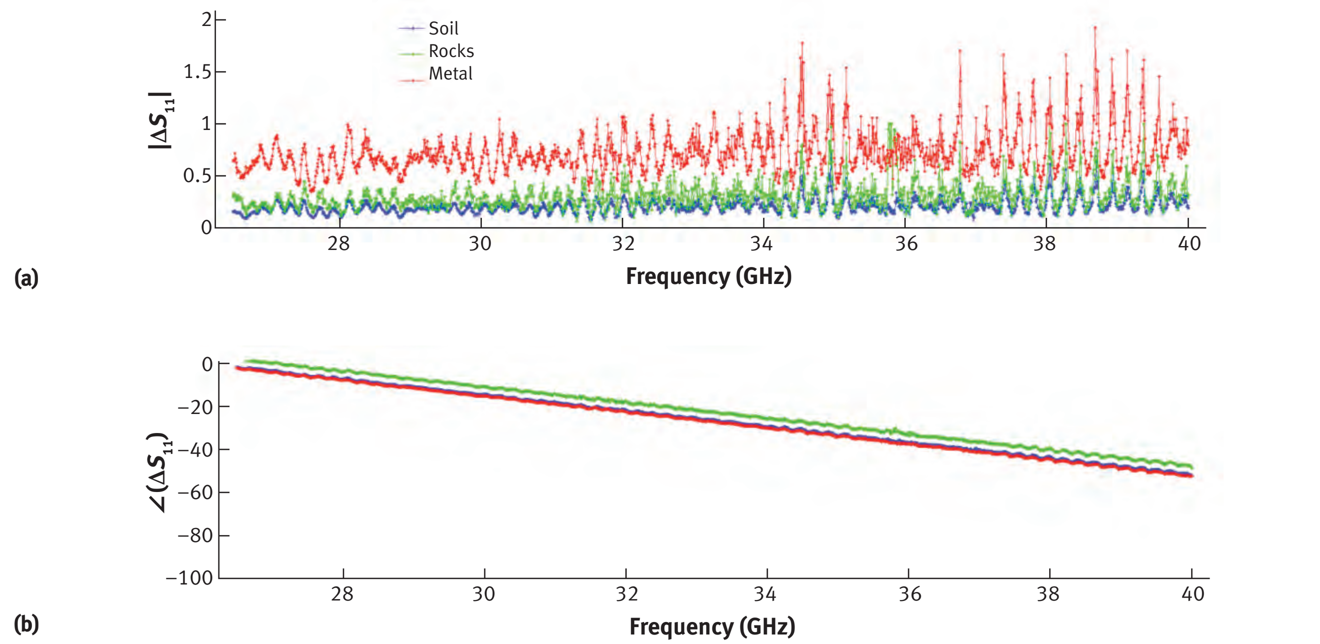


**Figure 7. Experimental $S$-parameter contrast $\Delta S_{11} \equiv S_{11} - S_{11}$ (water) for different materials in the middle layer of the sandwich structure, that is, soil, rocks and metal: (a) amplitude; and (b) phase.**

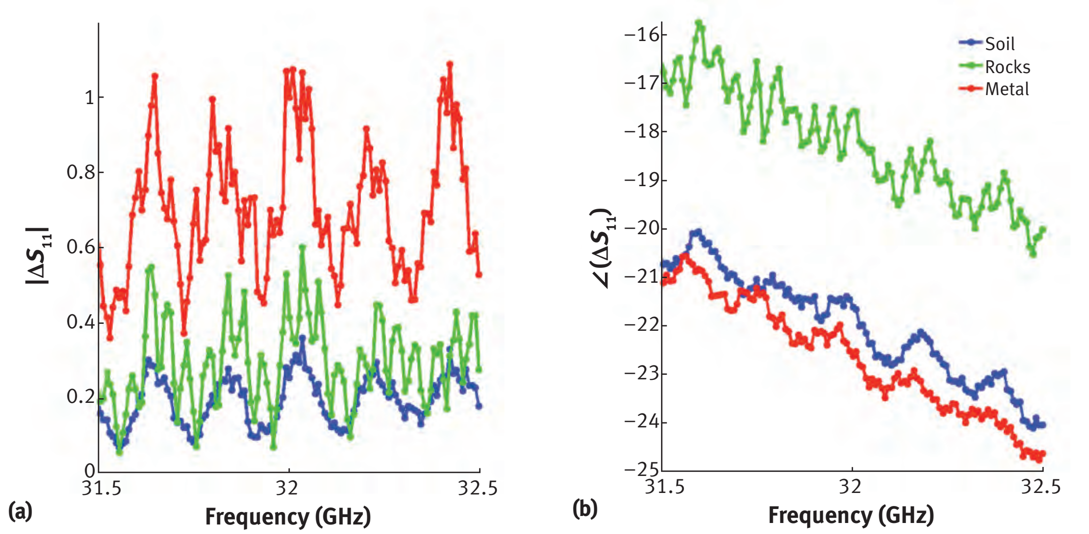


**Figure 8. A snapshot of Figure 6 showing the details over a narrow frequency range.**

## Discussion

The feasibility of standoff through-wall sensing of different materials at the Ka-band was demonstrated using a wide-band, stepped-frequency measurement approach. Both theoretical and experimental results show promise for application of this technique to TWI at these relatively high microwave frequencies for high-resolution imaging of hidden objects (for example, those covered by wall, soil or snow). The detection range can be estimated by the Friis transmission equation as:

$$P_d(\text{min.}) = P_t G^2 \left(\frac{\lambda}{4\pi R}\right)^2 \quad (7)$$
$$\Rightarrow R = \lambda \frac{G}{4\pi}\sqrt{\frac{P_t}{P_d(\text{min.})}}$$

where

$R$ is the range,

$P_t$ and $P_d$ (min.) are the transmitted and the minimum detectable power by the system, respectively,

$\lambda$ is the operating wavelength,

$G$ is the gain of the system.

Future extension of this monostatic setup to mobile systems with multiple antennas (array configuration) is expected to provide even higher resolution for 2D TWI applications. If combined with a frequency sweeping function, 3D TWI is also possible, allowing identification of objects behind a wall with known dielectric constant and thickness (Ahmad et al., 2008).

## Conclusion

Through-wall sensing of various materials at the Ka-band have been investigated using a monostatic, stepped-frequency experimental setup. A network analyzer was used to measure the $S$-parameter, $S_{11}$, of an object within a layered structure over the frequency range of 26.5 to 40 GHz. The target in this work was a wall block/object/wall block sandwich structure. The hidden objects in the middle layer included water, soil, rocks and metal. The combined amplitude and phase information of the reflected signal shows clear contrast among various objects sandwiched between two wall blocks. Theoretical calculations based on a plane wave solution obtained using a boundary matching technique were also performed. Numerical results showed good agreement with the experimental data. The results of this investigation suggest that high-resolution mmW through-wall sensing and TWI techniques could provide a viable alternative to low-frequency microwave TWI.

### AUTHORS

**S. Liao:** Argonne National Laboratory, 9700 S. Cass Ave., Argonne, Illinois 60439; e-mail sliao@anl.gov.

**T. Elmer:** Argonne National Laboratory, 9700 S. Cass Ave., Argonne, Illinois 60439.

**S. Bakhtiari:** Argonne National Laboratory, 9700 S. Cass Ave., Argonne, Illinois 60439.

**N. Gopalsami:** Argonne National Laboratory, 9700 S. Cass Ave., Argonne, Illinois 60439.

**N. Cox:** Argonne National Laboratory, 9700 S. Cass Avenue, Ave., Argonne, Illinois 60439.

**J. Wiencek:** Argonne National Laboratory, 9700 S. Cass Avenue, Ave., Argonne, Illinois 60439.

**A.C. Raptis:** Argonne National Laboratory, 9700 S. Cass Avenue, Ave., Argonne, Illinois 60439.

### REFERENCES

Aamna, M., S. Ammar, T. Rameez, S. Shabeeb, N.I. Rao and I. Safwat, "2D Beamforming for Through-the-wall Microwave Imaging Applications," *2010 International Conference on Information and Emerging Technologies*, 14–16 June 2010, Karachi, Pakistan.

Aftanas, M., "Signal Processing Steps for Objects Imaging through the Wall with UWB Radar," *9th Scientific Conference of Young Researchers*, Kosice, Slovakia, May 2009.

Aftanas, M., E. Zaikov, M. Drutarovsky and J. Sachs, "Through Wall Imaging of the Objects Scanned by M-sequence UWB Radar System," *Proceedings of the 18th International Conference Radioelektronika*, Prague, Czech Republic, April 2008, pp. 33–36.

Ahmad, F., Y. Zhang and M.G. Amin, "Three-dimensional Wideband Beamforming for Imaging through a Single Wall," *IEEE Geoscience and Remote Sensing Letters*, Vol. 5, No. 2, April 2008.

Bakhtiari, S., N. Gopalsami and A.C. Raptis, "Characterization of Delamination and Disbonding in Stratified Dielectric Composites by Millimeter Wave Imaging," *Materials Evaluation*, Vol. 53, No. 4, 1995, pp. 468–471.

Bakhtiari, S., N. Qaddoumi, S. Ganchev and R. Zoughi, "Microwave Non-contact Examination of Disbond and Thickness Variation in Stratified Composite Media," *IEEE Transactions on Microwave Theory and Technology*, Vol. 42, No. 3, 1994.

Bois, K., A. Benally and R. Zoughi, "Microwave Near-field Reflection Property Analysis of Concrete for Material Content Determination," *IEEE Transactions on Instrumentation and Measurement*, Vol. 49, No. 1, 2000, pp. 49–55.

Botros A.Z., A.D. Olver, L.G. Cuthbert and G. Farmer, "Microwave Detection of Hidden Objects in Walls," *Electronics Letters*, Vol. 20, No. 9, 1984, pp. 379–380.

Chen, K. M., Y. Huang, J. Zhang and A. Norman, "Microwave Life-detection Systems for Searching Human Subjects under Earthquake Rubble or behind Barrier," *IEEE Transactions on Biomedical Engineering*, Vol. 27, 2000, pp. 105–114.

Dehmollaian, M. and K. Sarabandi, "Simulation of Through-wall Microwave Imaging: Forward and Inverse Models," *IEEE International Symposium on Geoscience and Remote Sensing Symposium*, 2006.

D'Urso, M., G. Leone and F. Soldovieri, "A Simple Strategy for Life Signs Detection via an X-band Experimental Set-up," *Progress In Electromagnetics Research C*, Vol. 9, 2009, pp. 119–129.

Jackson, J.D., *Classical Electrodynamics*, 3rd ed., Wiley, Hoboken, New Jersey, 1998.

Johnson, J.T., M.A. Demir and N. Majurec, “Through-wall Sensing with Multifrequency Microwave Radiometry: a Proof-of-concept Demonstration,” *IEEE Transactions on Geoscience and Remote Sensing*, Vol. 47, No. 5, May 2009, pp. 1281–1288.

Liao, S., N. Gopalsami, A. Heifetz, T. Elmer, P. Fiflis, E.R. Koehl, H.T. Chien and A.C. Raptis, “Microwave Remote Sensing of Ionized Air,” *IEEE Geoscience and Remote Sensing Letters*, Vol. 8, No. 4, July 2011.

Lubecke, V.M., O. Boric-Lubecke, A. Host-Madsen and A.E. Fathy, “Through-the-wall Radar Life Detection and Monitoring,” Proceedings of 2007 Microwave Symposium, Honolulu, Hawaii, 3–8 May 2007, pp. 769–772.

Mubarak, K., K.J. Bois and R. Zoughi, “A Simple, Robust and On-site Microwave Technique for Determining Water-to-cement (w/c) Ratio of Fresh Portland Cement-based Materials,” *IEEE Transactions on Instrumentation and Measurement*, Vol. 50, No. 5, 2001, pp. 1255–1263.

Pieraccini, M., G. Luzi, D. Dei, L. Pieri and C. Atzeni, “Detection of Breathing and Heartbeat through Snow using a Microwave Transceiver,” *IEEE Geoscience and Remote Sensing Letters*, Vol. 5, No. 1, 2008, pp. 57–59.

Sen M.K., P.L. Stoffa, R.K. Seifoullaev and J.T. Fokkema, “Numerical and Field Investigations of GPR: Toward an Airborne GPR,” *Subsurface Sensing Technologies and Applications*, Vol. 4, No. 1, 2003.

Yemelyanov, K.M., N. Engheta, A. Hoorfar and J.A. McVay, “Adaptive Polarization Contrast Techniques for Through-wall Microwave Imaging Applications,” *IEEE Transactions on Geoscience and Remote Sensing*, Vol. 47, No. 5, 2009, pp. 1362–1374.

Zhuravlev A., A. Bugaev, S. Ivashov, V. Razevig and I. Vasiliev, “Microwave Holography in Detection of Hidden Objects under the Surface and Beneath Clothes,” *URSI General Assembly and Scientific Symposium*, 2011, pp. 1–4.

Zoughi, R., S. Gary and P.S. Nowak, “Microwave Nondestructive Estimation of Cement Paste Compressive Strength,” *ACI Materials Journal*, Vol. 92, No. 1, 1995, pp. 64–70.